CrossMark

No Need for Extreme Stellar Masses at $z \sim 7$: A Test-case Study of COS-87259

Sophie E. van Mierlo[1] 📧, Karina I. Caputi[1,2] 📧, and Vasily Kokorev[1] 📧
[1] Kapteyn Astronomical Institute, University of Groningen, PO Box 800, 9700 AV Groningen, The Netherlands; mierlo@astro.rug.nl
[2] Cosmic Dawn Center (DAWN), Denmark

Abstract

Recent controversy regarding the existence of massive ($\log(M_*/M_\odot) \gtrsim 11$) galaxies at $z > 6$ poses a challenge for galaxy formation theories. Hence, it is of critical importance to understand the effects of SED fitting methods on stellar mass estimates of Epoch of Reionization galaxies. In this work, we perform a case study on the AGN host galaxy candidate COS-87259, with spectroscopic redshift $z_{\rm spec} = 6.853$, that is claimed to have an extremely high stellar mass of $\log(M_*/M_\odot) \sim 11.2$. We test a suite of different SED fitting algorithms and stellar population models on our independently measured photometry in 17 broad bands for this source. Between five different code setups, the stellar mass estimates for COS-87259 span $\log(M_*/M_\odot) = 10.24–11.00$, while the reduced χ^2 values of the fits are all close to unity within $\Delta\chi^2_\nu = 1.2$, such that the quality of the SED fits is basically indistinguishable. Only when we adopt a nonparametric star formation history model within PROSPECTOR do we retrieve a stellar mass exceeding $\log(M_*/M_\odot) = 11$. Although the derived stellar masses change when using previously reported photometry for this source, the nonparametric SED-fitting method always yields the highest values. As these models are becoming increasingly popular for James Webb Space Telescope high-redshift science, we stress the absolute importance of testing various SED fitting routines particularly on apparently very massive galaxies at such high redshifts.

Unified Astronomy Thesaurus concepts: High-redshift galaxies (734); Stellar masses (1614); Spectral energy distribution (2129)

1. Introduction

Over the past two decades, many examples of galaxies with stellar masses $\log(M_*/M_\odot) \gtrsim 11$ out to redshift $z \sim 6$ have been found (e.g., Caputi et al. 2011; Stefanon et al. 2015; Deshmukh et al. 2018; Marsan et al. 2022). However, toward the Epoch of Reionization (EoR; $z \gtrsim 6$), such massive galaxies become increasingly rarer (e.g., Stefanon et al. 2021). For instance, Caputi et al. (2015) found virtually no galaxy with stellar mass $\log(M_*/M_\odot) > 11.0$ at such high redshifts over $0.8 \deg^2$ within the COSMOS field (Scoville et al. 2007). This result has been recently challenged by the apparent discovery of unusually massive galaxies at $z > 6$ (Endsley et al. 2022b; Labbe et al. 2022). The existence of these sources would be in tension with galaxy formation theories assuming ΛCDM cosmology (e.g., Behroozi & Silk 2018; Boylan-Kolchin 2022; Menci et al. 2022).

Galaxy stellar masses are usually estimated through spectral energy distribution (SED) fitting of photometric data. Many different SED fitting codes exists, which can lead to significantly different stellar mass estimates of the same object, especially for apparently faint galaxies (e.g., Dahlen et al. 2013; Weaver et al. 2022). Therefore, a critical study of the effects of SED fitting approaches on the derived stellar masses at $z > 6$ is of utmost importance.

For example, recent works have demonstrated that SED models assuming a nonparametric star formation history (SFH) yield higher stellar masses compared to traditional parametric descriptions (Tacchella et al. 2022; Topping et al. 2022; Whitler et al. 2022), although Stefanon et al. (2022) found

identical stellar masses between a constant and nonparametric SFH fit of a stacked sample of $z \sim 10$ galaxies. In addition, the choice of initial mass function (IMF) also affects the derived stellar mass, and a Galactic IMF might not be the most suitable at $z > 6$ (Steinhardt et al. 2022).

In this letter, we present a case study of the source COS-87259, located in the third ultra-deep stripe of the UltraVISTA survey in COSMOS. This galaxy was originally identified as a $z_{\rm phot} \approx 6.6–6.9$ Lyman-break galaxy in Endsley et al. (2021). Subsequently, Endsley et al. (2022a) identified radio and X-ray emission coming from this source, concluding that this galaxy likely harbors an active galactic nucleus (AGN). Finally, Endsley et al. (2022b) conducted follow-up spectroscopy with ALMA, identifying strong [CII]158 μm and dust continuum emission, establishing a precise spectroscopic redshift of $z_{\rm phot} = 6.853 \pm 0.002$. Endsley and collaborators obtained different stellar mass estimates for COS-87259 in their different works, with the study based on optical to far-infrared photometry including the ALMA measurement claiming that its best-estimate stellar mass is $\log(M_*/M_\odot) = 11.2 \pm 0.2$.

By using different SED fitting codes, in this work we assess whether this extremely high stellar mass value is necessarily the most accurate estimate for COS-87259. We adopt a cosmology with $H_0 = 70 \text{ km s}^{-1} \text{ Mpc}^{-1}$, $\Omega_m = 0.3$, and $\Omega_\Lambda = 0.7$. All magnitudes and fluxes are total, with magnitudes referring to the AB system (Oke & Gunn 1983). Stellar masses correspond to a Chabrier (2003) IMF.

2. Photometry

COS-87259 is part of the UltraVISTA ultra-deep catalog presented in van Mierlo et al. (2022). Based on the photometry in this catalog, our initial photometric redshift for COS-87259 is $z_{\rm phot} = 6.87^{+0.08}_{-0.07}$, in excellent agreement with the

spectroscopic redshift from Endsley et al. (2022b). To obtain more precise flux measurements for this analysis, we redid the photometry for COS-87259, using the PYTHON modules ASTROPY (version 5.0.4; Astropy Collaboration et al. 2022) and PHOTUTILS (version 1.4.1; Bradley et al. 2022).

We included ultra-deep optical data from Data Release (DR) 3 of the Subaru Hyper Suprime-Cam (HSC) Strategic Program (Aihara et al. 2022) in the g, r, i, z, and y bands. In addition, we consider CFHT Megacam u and Subaru Suprime-Cam broadband data, namely the B, V, r^+, i^+, and z^{++} bands (Ilbert et al. 2009; Taniguchi et al. 2015). We also included the UltraVISTA DR4 VIRCAM Y, J, H, and K_s data (McCracken et al. 2012) and IRAC 3.6 and 4.5 μm imaging from the SMUVS program (Ashby et al. 2018; Deshmukh et al. 2018). In total, we consider imaging in 17 rest-frame optical to near-infrared (NIR) broad bands, which together probe the rest-frame wavelength range 450–6390 Å at $z_{spec} = 6.853$.

We measured the photometry in $2''$ circular diameters at the position of COS-87259 measured from the HK_s stack, i.e., R.A. $\alpha = 149^h44^m34^s06$ and decl. $\delta = +01^d39^m20^s10$. COS-87259 has only two faint low-redshift neighbors in a $5''$ radius that are both undetected in IRAC, such that we are not worried about flux contamination. Assuming a point-source morphology, aperture flux corrections were derived for each band individually, using the curves of growth of nearby bright stars, and used to correct the fluxes to total.

To derive the flux errors in all but the IRAC bands, we measured the background fluxes in $2''$ empty apertures over a $30''$ by $30''$ region around the source, and calculated the flux error as the standard deviation of the flux distribution that was 3σ-clipped over five iterations. As the IRAC images suffer from source confusion, for the IRAC flux errors we instead adopted a SOURCEEXTRACTOR-like approach (Bertin & Arnouts 1996), meaning that we derive the flux errors from the local background measurement in a $4''$–$8''$ diameter annulus surrounding the source.

Finally, all fluxes and error measurements were corrected for Galactic dust extinction using the Schlafly & Finkbeiner (2011) dust maps with the Fitzpatrick (1999) reddening law. In bands with nondetections, we adopt 3σ flux upper limits derived from the empty aperture fluxes. We present an overview of our flux measurements in each band in Table 1.

We compare our photometric measurements of COS-87259 to those by Endsley et al. (2022a), presented in their Table 1. Between the bands that overlap in both samples, our flux upper limits in nondetected bands are systematically lower, by at most a factor $\sim$6 in HSC g. Our VISTA Y, J, and H measurements all agree within the flux uncertainty, but most importantly, our $K_s - [3.6]$ color of 0.9 is significantly bluer than the $K_s - [3.6] = 1.5$ from Endsley et al. (2022a). In Section 4, we demonstrate how the photometric differences between our work and theirs affect our stellar mass comparison for COS-87259.

3. SED Fitting

In this section, we describe the different SED fitting approaches we took to derive the physical properties of COS-87259. We ran each code on the 17 band photometry, with the redshift fixed to the spectroscopic redshift $z_{spec} = 6.853$ from Endsley et al. (2022b).

Table 1
Optical and NIR Flux Density Measurements for COS-87259, as Obtained in This Work

Telescope/Instrument	Band	Flux (μJy)
CFHT/MegaCam	u	<0.0039
Subaru/Suprime-Cam	B	<0.0050
Subaru/HSC	g	<0.0045
Subaru/Suprime-Cam	V	<0.014
Subaru/HSC	r	<0.0067
Subaru/Suprime-Cam	r^+	<0.013
Subaru/Suprime-Cam	i^+	<0.013
Subaru/HSC	i	<0.0079
Subaru/HSC	z	<0.0098
Subaru/Suprime-Cam	z^{++}	0.007 ± 0.025
Subaru/HSC	y	0.097 ± 0.053
VISTA/VIRCAM	Y	0.214 ± 0.035
VISTA/VIRCAM	J	0.391 ± 0.043
VISTA/VIRCAM	H	0.577 ± 0.051
VISTA/VIRCAM	K_s	0.837 ± 0.081
Spitzer/IRAC	[3.6]	1.90 ± 0.17
Spitzer/IRAC	[4.5]	1.91 ± 0.18

Note. For nondetections, 3σ upper limits are reported.

3.1. LePhare with BC03

As a first code, we used the traditional, well-tested algorithm LEPHARE (Arnouts et al. 1999; Ilbert et al. 2006). The galaxy models were sampled from the GALAXEV library (Bruzual & Charlot 2003; BC03 hereafter).

We adopted different SFHs: a single stellar population and two parametric SFHs, i.e., an exponentially declining SFH (SFR $\propto e^{-t/\tau}$) and a delayed exponentially declining (SFR $\propto te^{-t/\tau}$), using star formation timescales $\tau = 0.01$, 0.1, 0.3, 1.0, 3.0, 5.0, 10.0, and 15 Gyr. We considered solar ($Z = Z_\odot$) and subsolar ($Z = 0.2Z_\odot$) metallicities.

We adopted the Calzetti et al. (2000) reddening law and left the color excess free between $E(B - V) = 0$–1. Emission lines were incorporated following the scaling relations from Kennicutt, Jr (1998) (see Ilbert et al. 2009 for a detailed description). Absorption of emission at wavelengths shorter than rest-frame 912 Å by the intergalactic medium (IGM) was implemented following Madau (1995). LEPHARE rejects any modeled SED that produces fluxes higher the 3σ upper limits in the nondetected bands.

3.2. LePhare with STARBURST99

Young galaxies with strong nebular line and continuum emission can have significantly boosted broadband flux measurements, such that their stellar masses may be overestimated by up to a factor of 10 (Bisigello et al. 2019). Therefore, we performed a separate SED fitting run with LEPHARE using stellar population models from the STARBURST99 library (Leitherer et al. 1999), which include both stellar emission and nebular line and continuum emission. We considered five templates with subsolar metallicity of $Z = 0.05Z_\odot$, ages spanning 10^6–10^8 yr, and constant SFRs between 0.01 and 10 $M_\odot yr^{-1}$. These templates were compiled into SED models and fitted to the photometry following the LEPHARE approach described in Section 3.1.

3.3. Prospector

The second code we considered is the Bayesian inference code PROSPECTOR (Johnson et al. 2021). This relatively new code has been extensively tested on low-redshift galaxies (e.g., Leja et al. 2017, 2019), but more recently it has been used in numerous works to model the properties of very high-redshift galaxies, including James Webb Space Telescope (JWST)-observed sources (e.g., Naidu et al. 2022; Tacchella et al. 2022; Whitler et al. 2022).

PROSPECTOR uses the Flexible Stellar Population Synthesis code (FSPS; Conroy et al. 2009; Conroy & Gunn 2010). We tested both a delayed exponentially declining SFH and a flexible, nonparametric SFH.

Our parametric model involves six free parameters, using the default prior shapes with the following ranges: the formed stellar mass $M_* = 10^9$–$10^{12} M_\odot$, the metallicity $\log(Z/Z_\odot) = -2$–0.19, the e-folding time $\tau_{SF} = 0.001$–$15 \, Gyr$, and the age $t_{age} = 0.001$–$13.8 \, Gyr$. We modeled diffuse dust attenuation following Calzetti et al. (2000) with $\tau_{dust} = 0$–4. Finally, we implemented IGM absorption following Madau (1995) and nebular emission using the default parameters.

In the nonparametric model ("continuity prior"), the SFH history is described by N temporal bins, with a constant SFR in each bin, and PROSPECTOR fits the ratio between these bins. We largely adopted the approach outlined in Tacchella et al. (2022), modeling six time bins, where the first bin spans 0–10 Myr in lookback time and the remaining five bins are spaced equally in logarithmic time space up to $z = 20$. In addition, we fitted the formed stellar mass, metallicity, diffuse dust attenuation, IGM absorption factor, and gas ionization parameter, following the PROSPECTOR parametric model.

Finally, PROSPECTOR treats nondetections by utilizing the 1σ flux limit as the flux error.

3.4. EAZY

As a third SED fitting model, we used the PYTHON version of EAZY (Brammer et al. 2008). EAZY utilizes a series of non-negative linear combinations of basis-set templates constructed with the FSPS models. Specifically, we used the CORR_SFHZ_13 subset of models within EAZY. These models contain redshift-dependent SFHs, which, at a given redshift, exclude the SFHs that start earlier than the age of the universe. The maximum allowed attenuation is also tied to a given epoch. Additionally, we included the best-fit template to the JWST-observed extreme emission line galaxy at $z = 8.5$ (ID4590) from Carnall et al. (2023), which has been rescaled to match the normalization of the FSPS models. This was done to adequately model potential emission lines with large equivalent widths.

To fit our object, we adopted the EAZY template error function, to account for any additional uncertainty related to unusual stellar populations, using the default value of 0.2 for the template error. For nondetected bands, EAZY utilizes the 1σ flux upper limit in the fit.

4. Results

Here, we compare the best-fit SEDs and associated stellar masses of COS-87259 obtained with the approaches outlined in Section 3.

Table 2
Resulting Fit Parameters from Various SED Fitting Runs on the Optical to NIR Broadband Photometry of COS-87259

Code	Stellar Population Models	SFH	χ^2_ν	M_* (log[$M/M_\odot$])
LePhare	BC03	Parametric	0.66	$10.42^{+0.22}_{-0.05}$
Prospector	FSPS	Parametric	1.11	$11.00^{+0.05}_{-0.07}$
Prospector	FSPS	Binned SFH	2.20	$11.16^{+0.06}_{-0.05}$
LePhare	STARBURST99	Parametric	1.19	$10.24^{+0.18}_{-0.05}$
EAZY	FSPS/Carnall et al. (2023)	Parametric	1.55	$10.53^{+0.09}_{-0.12}$

For each SED fitting code and choice of stellar population models, we report the reduced χ^2 and stellar mass in Table 2. The corresponding best-fit SEDs are shown in Figure 1. Each code has its own metric to determine the best-fit SED, so we explain them as follows. With LEPHARE, the best-fit SED simply minimizes the χ^2 value compared to the observed photometry, and the stellar mass uncertainties reflect the 34th and 66th percentiles of the maximum likelihood distribution. The resulting SEDs and stellar masses obtained with PRO-SPECTOR correspond to the median of the posterior SED, and the errors on the stellar represent the 34th and 66th percentiles of the stellar mass posterior distribution. Finally, EAZY returns the best-fit SED based on the linear combination of templates that maximizes the posterior probability distribution, with the errors on the stellar mass derived as the 16th and 84th percentiles. The nonhomogeneous error recipes between the codes should be taken into account account upon comparing the stellar mass errors in Table 2, as it makes our reported EAZY stellar mass error inherently larger.

To compare the goodness of fit for each model, we use the reduced χ^2 metric calculated from comparing the observed and modeled photometry (including contribution from emission lines) in all bands, excluding flux upper limits, where the number of degrees of freedom is simply the number of secure detections minus one, i.e., seven (see Table 1). For the stellar mass estimates presented in Table 2, we imposed a minimum error of 0.05 (10σ), which was derived from the signal-to-noise ratio in the observed band that samples the SED most closely to the rest-frame K-band, i.e., the IRAC 4.5 μm band. At $z \sim 7$, the IRAC 4.5 μm band samples the rest-frame $\sim$5500 Å continuum and should be free from strong emission lines, such that it provides the best assessment of the stellar mass uncertainty given the our photometric data set for this source.

Our most important result is that, between the five setups of codes and stellar population models, the resulting stellar masses differ by up to 0.9 dex, whereas it is virtually impossible to determine which of these fits is most representative of the truth: the χ^2_ν values are all close to one and differ by 1.54 at most.

Between the runs performed with LEPHARE using the BC03 models and the PROSPECTOR parametric setup, their best-fit SEDs shown in Figure 1(a) and 1(b), respectively; the stellar masses differ by 0.6 dex and do not agree within the errors, even though we chose the run parameters to be as similar as possible. We believe this is partially because of the different templates sets, but also because of the actual SED fitting prescriptions (even if the stellar mass is derived directly from the template normalization), given that stellar mass difference
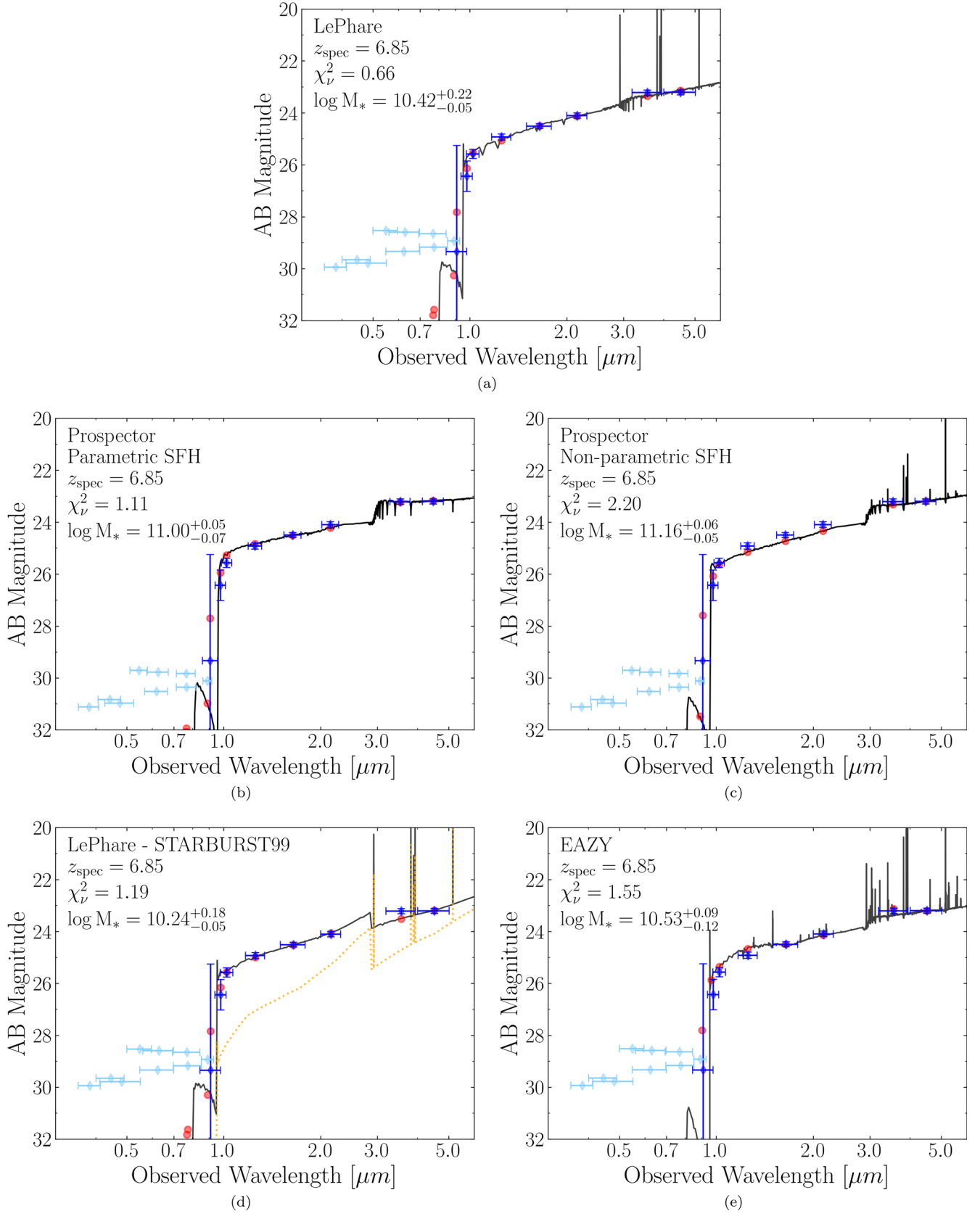
Figure 1. Best-fit SEDs corresponding to the five SED fitting setups presented in Table 2. In each panel, the SED is shown in a black line. The observed fluxes and flux upper limits are shown in dark and light blue diamonds, respectively. The template fluxes in each band are shown in red points. Each panel reports the SED fitting setup, the spectroscopic redshift from Endsley et al. (2022b), the reduced χ^2 value of the fit, and the stellar mass. For the LEPHARE run using STARBURST99 models, shown in the lower left panel, the yellow dotted line represents the contribution of nebular emission to the total SED.

4

between the LEPHARE+BC03 and LEPHARE+STARBURST99 runs is only 0.18 dex.

According to the LEPHARE+BC03 result, this galaxy would be of solar metallicity, young at 0.01 Gyr old, actively undergoing star formation with $\tau = 15$ Gyr, and quite dusty with $A_V = 2.03$. Instead, PROSPECTOR finds that this source would be metal-poor with $Z = 0.014 Z_\odot$, relatively old with an age of 0.18 Gyr, and less dusty with $A_V = 0.80$. Most importantly, its SFH e-folding time of only 0.003 Gyr and lack of nebular emission lines suggest that this galaxy would have undergone a short burst of SF upon creation and evolved relatively passively afterward. Based on the χ^2_ν values of these different fits, it is impossible to say with confidence which result is more likely between these two conflicting descriptions of COS-87259's nature.

Using PROSPECTOR, we explicitly assess the dependency of stellar mass on the assumed SFH. We find a moderate difference of 0.12 dex in stellar mass between the two models, such that the stellar mass of $\log(M_*/M_\odot) = 11.16$ from the nonparametric SFH exceeds the parametric estimate of $\log(M_*/M_\odot) = 11.00$, even within the uncertainty. This effect has been observed in other works at similar redshift (Topping et al. 2022; Whitler et al. 2022). The nonparametric fit has the highest associated $\chi^2_\nu = 2.20$, explained by the underestimation of rest-frame UV fluxes due to moderate dust attenuation of $A_V = 1.44$. When we inspect our nonparametric SFH fit, we find that more than 80 % of the stellar mass was formed between lookback times of 0.18 Gyr and 0.042 Gyr, with a constant SFR of 1166 $M_\odot$ yr^{-1}. After this initial burst, the star formation rate falls off and continues at 42 $M_\odot$ yr^{-1}. This could explain the slightly higher stellar mass as compared to the parametric SFH, for which star formation ceases completely in the last $\sim 10^7$ yr.

We find that the stellar mass estimate from LEPHARE using the STARBURST99 templates is the lowest of our considered setups, at $\log(M_*/M_\odot) = 10.24$ with $\chi^2_\nu = 1.19$. The best-fit SED is shown in Figure 1(d), and corresponds to a 0.01 Gyr old galaxy with a constant SFR of 10 $M_\odot$ yr^{-1} and subsolar metallicity $Z = 0.05 Z_\odot$. Upon decomposition of the SED, we find that 52 % of the integrated light is in fact nebular emission, resulting in a corrected stellar mass of only $\log(M_*/M_\odot) = 9.91$.

Finally, we show the best-fit SED obtained with EAZY in Figure 1(e). The stellar mass from this fit is $\log(M_*/M_\odot) = 10.53$, with an associated $\chi^2_\nu = 1.55$, which makes the EAZY SED the worst fit out of the five code setups considered here. EAZY identifies COS-87259 as a 0.05 Gyr old galaxy with moderate dust content, such that $A_V = 0.87$, and a strong presence of emission lines.

We have demonstrated how different SED fitting approaches applied to independent photometric data produce strongly varying stellar mass estimates for COS-87259. Moreover, our estimates are all lower than the $\log(M_*/M_\odot) = 11.2 \pm 0.2$ value from Endsley et al. (2022b), although, given the uncertainty on their stellar mass estimate, it is not significantly different from our PROSPECTOR results.

The stellar mass discrepancy might to some extent be explained by different photometric values: we measure a significantly bluer $K_s - [3.6] = 0.9$ color than $K_s - [3.6] = 1.5$ from Endsley et al. (2022a). At $z \sim 7$, the $K_s - [3.6]$ color is sensitive to the 4000 Å break, but also to O[III] + Hβ emission, which can boost the IRAC 3.6 μm flux.

As a sanity check, we have run all codes discussed in Section 3 on the optical and NIR photometry (HSC g up to IRAC 4.5μm) from Table 1 in Endsley et al. (2022a), again fixing the redshift to $z_{\rm spec} = 6.853$. With our LEPHARE+BC03 setup, we retrieve a stellar mass estimate of $\log(M_*/M_\odot) = 10.87^{+0.16}_{-0.13}$. This is 0.45 dex higher than the LEPHARE+BC03 stellar mass derived from our own photometry, and the values do not agree within the error bars. Surprisingly, the HSC IB945 flux upper limit strongly affects the stellar mass: if we change the significance of this constraint from 2σ to 3σ, the best-fit SED changes to a $\log(M_*/M_\odot) = 10.58^{+0.15}_{-0.10}$ result. Furthermore, from our other code setups, we retrieve systematically higher stellar masses for COS-87259, compared to our own results, but the same spread in masses of 0.9 dex. Therefore, we conclude that our lower stellar mass estimate for COS-87259 is partially driven by our photometry, but the discrepancies between the results of our considered SED fitting routines are not.

5. Combined Stellar and Dust Emission SED Fitting

Another key difference with respect to our analysis that could explain the $\log(M_*/M_\odot) = 11.2 \pm 0.2$ result from Endsley et al. (2022b) is the inclusion of FIR to millimeter data, especially given that COS-87259 likely harbors an AGN. In fact, Endsley et al. (2022b) have fitted the full optical to millimeter wavelength photometry with a custom Bayesian SED fitting package, which includes AGN and galaxy dust emission components, as well as stellar emission using the FSPS code under the PROSPECTOR framework. So far, we have only fitted the optical to NIR regime, so here we adopted the 5.8 μm to 1.4 mm photometry for COS-87259 from Endsley et al. (2022b) and Table 1 in Endsley et al. (2022a).

This combined suite of photometry is fitted with the SED-fitting code STARDUST (Kokorev et al. 2021), again fixing the redshift to $z_{\rm spec} = 6.853$. STARDUST models light from stars and AGN, as well as infrared emission arising from the dust reprocessed stellar continuum. Similarly to EAZY, STARDUST fits independent linear combinations of templates, but with the key advantage of not assuming the energy balance between stellar and dust emission. For our fit, we utilized UV-NIR templates adopted from EAZY, empirically derived AGN templates from Mullaney et al. (2011), and the dust models from Draine & Li (2007). For the latter, the minimum radiation fields intensity spans $U_{\rm min} = 40$–50, and the fraction of dust contained in the photodissociation regions spans $\gamma = 0.01$–0.3. When combined, these correspond to a range of luminosity-weighted dust temperatures ($T_{\rm dust}$) from 35 to 45 K.

The best-fit SED obtained from STARDUST is shown in Figure 2. We note that STARDUST treats any flux measurement with a confidence level $<3\sigma$ as an upper limit instead, which brings the the total number of secure detections to 14. The χ^2_ν value for this fit is 1.90, and the resulting stellar mass is $\log(M_*/M_\odot) = 10.81^{+0.05}_{-0.05}$, which is over 0.4 dex lower than the $\log(M_*/M_\odot) = 11.2 \pm 0.2$ stellar mass from Endsley et al. (2022b) and does not agree within the error bars. When we run STARDUST on the exact photometry from Endsley et al. (2022a), we retrieve a stellar mass of $\log(M_*/M_\odot) = 11.02^{+0.05}_{-0.05}$. These results with STARDUST reinforce our previous conclusion obtained with the SED fitting of only the source stellar emission: the stellar mass of COS-87259 is most likely $<10^{11.2} M_\odot$.
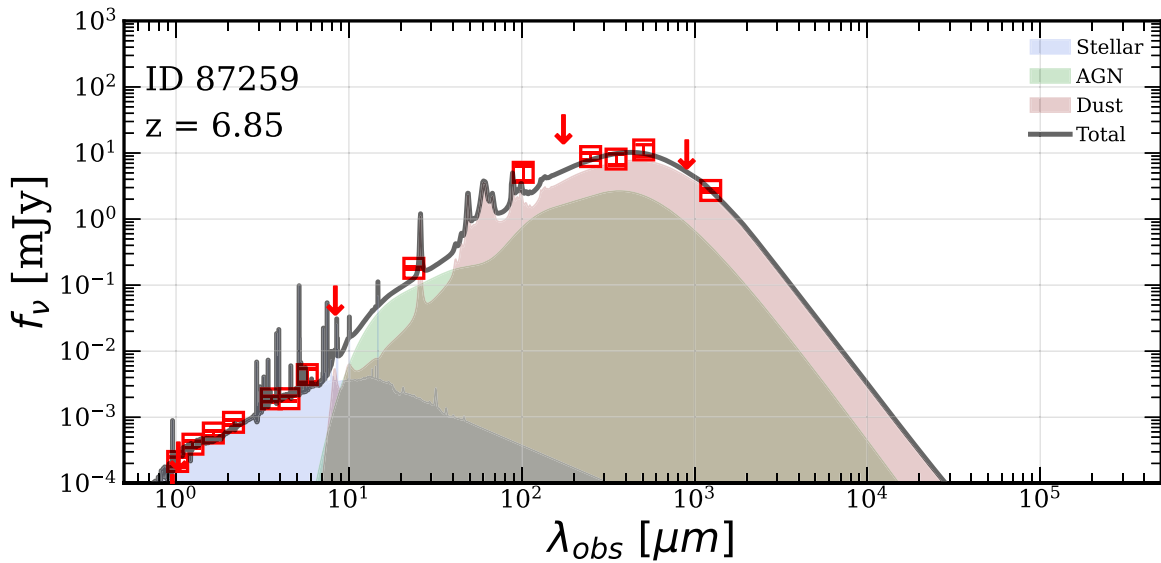
Figure 2. Best-fit SED of COS-87259 obtained with STARDUST on the observed UV to millimeter photometry from Endsley et al. (2022a) and Endsley et al. (2022b). The flux measurements are shown in red, where the arrows correspond to flux upper limits. The individual components of the stellar, AGN, and dust emission are shown in blue, green, and red curves respectively.

6. Conclusion

In this letter, we reassessed the stellar mass of $z_{\rm spec} = 6.853$ AGN host galaxy candidate COS-87259, located in the UltraVISTA ultra-deep region in the COSMOS field. This source has been extensively studied in previous works: its most recent stellar mass estimate is unexpectedly high, with $\log(M_*/M_\odot) = 11.2 \pm 0.2$ (Endsley et al. 2022b). Here, we took this galaxy as a case study to compare the best-fit SEDs and physical parameters obtained with different SED fitting routines. We measured independent photometry from 17 rest-frame optical to NIR broadband images for COS-87259. These data were fitted with SED fitting codes LEPHARE, PROSPECTOR, EAZY, and STARDUST, including 5.8 μm to 1.4 mm photometry from Endsley et al. (2022b) for the latter fit.

Between six setups of codes and stellar population models, we find that the resulting stellar masses span $\log(M_*/M_\odot) = 10.24$–11.16. Contrarily, the reduced χ^2 values of the fits are all close to unity within $\Delta\chi^2_\nu = 1.2$. Therefore, all SED fits are of comparable quality, making it virtually impossible to decide which stellar mass estimate is most representative of the truth.

We find that the combination of PROSPECTOR and a nonparametric description of the SFH (which has been frequently used to fit newly JWST-discovered high-redshift galaxies) yields the highest stellar mass estimate in this work, $\log(M_*/M_\odot) = 11.16$. Moreover, even when adopting a traditional parametric SFH, PROSPECTOR yields significantly higher stellar masses than any of the other considered codes. Finally, by considering very young galaxy templates that have strong nebular line and continuum emission, we obtain our lowest stellar mass estimate of $\log(M_*/M_\odot) = 10.24$ with $\chi^2_\nu = 1.19$.

We emphasize that none of our six considered SED fitting routines can replicate the extremely high stellar mass result from Endsley et al. (2022b), although this is partially explained by our bluer $K_{\rm s} - [3.6]$ color measurement. It should be noted however that a $\log(M_*/M_\odot) \geqslant 11$ solution for COS-87259 does not violate ΛCDM number density upper limit (Boylan-

Kolchin 2022), even when other $z \sim 7$ galaxies of such stellar masses may be discovered in the COSMOS field in the future (Lovell et al. 2023).

In conclusion, in light of the recent discoveries of very massive EoR galaxies with JWST, we emphasize the absolute importance of testing various SED fitting routines on these seemingly massive galaxies to obtain a confident stellar mass estimate. Otherwise, we may falsely conclude that JWST is allowing us to probe an unexpectedly numerous population of massive galaxies, whereas in fact overestimation from novel SED fitting approaches is the main driver behind these results. As for the specific instance of COS-87259, this source will be observed with JWST in the near future, hopefully bringing us yet again closer to a consensus on the nature of this undoubtedly interesting galaxy.

ORCID iDs

Sophie E. van Mierlo ⓘ https://orcid.org/0000-0001-8289-2863
Karina I. Caputi ⓘ https://orcid.org/0000-0001-8183-1460
Vasily Kokorev ⓘ https://orcid.org/0000-0002-5588-9156

References

Aihara, H., AlSayyad, Y., Ando, M., et al. 2022, PASJ, 74, 247
Arnouts, S., Cristiani, S., Moscardini, L., et al. 1999, MNRAS, 310, 540
Ashby, M. L. N., Caputi, K. I., Cowley, W., et al. 2018, ApJS, 237, 39
Astropy Collaboration, Price-Whelan, A. M., Lim, P. L., et al. 2022, ApJ, 935, 167
Behroozi, P., & Silk, J. 2018, MNRAS, 477, 5382
Bertin, E., & Arnouts, S. 1996, A&AS, 117, 393

Bisigello, L., Caputi, K. I., Colina, L., et al. 2019, ApJS, 243, 27
Boylan-Kolchin, M. 2022, arXiv:2208.01611
Bradley, L., Sipocz, B., Robitaille, T., et al. 2022, astropy/photutils:, v1.4.0, Zenodo, doi:10.5281/zenodo.6385735
Brammer, G. B., van Dokkum, P. G., & Coppi, P. 2008, ApJ, 686, 1503
Bruzual, G., & Charlot, S. 2003, MNRAS, 344, 1000
Calzetti, D., Armus, L., Bohlin, R. C., et al. 2000, ApJ, 533, 682
Caputi, K. I., Cirasuolo, M., Dunlop, J. S., et al. 2011, MNRAS, 413, 162
Caputi, K. I., Ilbert, O., Laigle, C., et al. 2015, ApJ, 810, 73
Carnall, A. C., Begley, R., McLeod, D. J., et al. 2023, MNRAS, 518, 45
Chabrier, G. 2003, PASP, 115, 763
Conroy, C., & Gunn, J. E. 2010, FSPS: Flexible Stellar Population Synthesis, Astrophysics Source Code Library, ascl:1010.043
Conroy, C., Gunn, J. E., & White, M. 2009, ApJ, 699, 486
Dahlen, T., Mobasher, B., Faber, S. M., et al. 2013, ApJ, 775, 93
Deshmukh, S., Caputi, K. I., Ashby, M. L. N., et al. 2018, ApJ, 864, 166
Draine, B. T., & Li, A. 2007, ApJ, 657, 810
Endsley, R., Stark, D. P., Chevallard, J., & Charlot, S. 2021, MNRAS, 500, 5229
Endsley, R., Stark, D. P., Fan, X., et al. 2022a, MNRAS, 512, 4248
Endsley, R., Stark, D. P., Lyu, J., et al. 2022b, arXiv:2206.00018
Fitzpatrick, E. L. 1999, PASP, 111, 63
Ilbert, O., Arnouts, S., McCracken, H. J., et al. 2006, A&A, 457, 841
Ilbert, O., Capak, P., Salvato, M., et al. 2009, ApJ, 690, 1236
Johnson, B. D., Leja, J., Conroy, C., & Speagle, J. S. 2021, ApJS, 254, 22
Kennicutt, R. C., Jr. 1998, ApJ, 498, 541
Kokorev, V. I., Magdis, G. E., Davidzon, I., et al. 2021, ApJ, 921, 40
Labbe, I., van Dokkum, P., Nelson, E., et al. 2022, arXiv:2207.12446

Leitherer, C., Schaerer, D., Goldader, J. D., et al. 1999, ApJS, 123, 3
Leja, J., Johnson, B. D., Conroy, C., et al. 2017, ApJ, 837, 170
Leja, J., Johnson, B. D., Conroy, C., et al. 2019, ApJ, 877, 140
Lovell, C. C., Harrison, I., Harikane, Y., Tacchella, S., & Wilkins, S. M. 2023, MNRAS, 518, 2511
Madau, P. 1995, ApJ, 441, 18
Marsan, Z. C., Muzzin, A., Marchesini, D., et al. 2022, ApJ, 924, 25
McCracken, H. J., Milvang-Jensen, B., Dunlop, J., et al. 2012, A&A, 544, A156
Menci, N., Castellano, M., Santini, P., et al. 2022, ApJL, 938, L5
Mullaney, J. R., Alexander, D. M., Goulding, A. D., & Hickox, R. C. 2011, MNRAS, 414, 1082
Naidu, R. P., Oesch, P. A., Dokkum, P. v., et al. 2022, ApJL, 940, L14
Oke, J. B., & Gunn, J. E. 1983, ApJ, 266, 713
Schlafly, E. F., & Finkbeiner, D. P. 2011, ApJ, 737, 103
Scoville, N., Aussel, H., Brusa, M., et al. 2007, ApJS, 172, 1
Stefanon, M., Bouwens, R. J., Labbe, I., et al. 2021, ApJ, 922, 29
Stefanon, M., Bouwens, R. J., Labbé, I., et al. 2023, ApJ, 943, 81
Stefanon, M., Marchesini, D., Muzzin, A., et al. 2015, ApJ, 803, 11
Steinhardt, C. L., Kokorev, V., Rusakov, V., Garcia, E., & Sneppen, A. 2022, arXiv:2208.07879
Tacchella, S., Finkelstein, S. L., Bagley, M., et al. 2022, ApJ, 927, 170
Taniguchi, Y., Kajisawa, M., Kobayashi, M. A. R., et al. 2015, PASJ, 67, 104
Topping, M. W., Stark, D. P., Endsley, R., et al. 2022, MNRAS, 516, 975
van Mierlo, S. E., Caputi, K. I., Ashby, M., et al. 2022, A&A, 666, A200
Whitler, L., Endsley, R., Stark, D. P., et al. 2023, MNRAS, 519, 157
Weaver, J. R., Kauffmann, O. B., Ilbert, O., et al. 2022, ApJS, 258, 11